Published in final edited form as:
J Am Chem Soc. 2007 May 9; 129(18): 5954–5961. doi:10.1021/ja069375w.

GM_1 Clustering Inhibits Cholera Toxin Binding in Supported Phospholipid Membranes

Jinjun Shi, **Tinglu Yang**, **Sho Kataoka**, **Yanjie Zhang**, **Arnaldo J. Diaz**, and **Paul S. Cremer***

Abstract

The present studies explore multivalent ligand–receptor interactions between pentameric cholera toxin B subunits (CTB) and the corresponding membrane ligand, ganglioside GM_1. CTB binding was monitored on supported phospholipid bilayers coated on the walls and floors of microfluidic channels. Measurements were made by total internal reflection fluorescence microscopy (TIRFM). Apparent dissociation constants were extracted by fitting the binding data to both the Hill–Waud and Langmuir adsorption isotherm equations. Studies of the effect of ligand density on multivalent CTB–GM_1 interactions revealed that binding weakened with increasing GM_1 density from 0.02 mol % to 10.0 mol %. Such a result could be explained by the clustering of GM_1 on the supported phospholipid membranes, which in turn inhibited the binding of CTB. Atomic force microscopy (AFM) experiments directly verified GM_1 clustering within the supported POPC bilayers.

Introduction

Multivalent ligand–receptor interactions are frequently utilized by nature because their properties can be remarkably different from the corresponding monovalent recognition events. For example, multivalent interactions can achieve tighter binding, enhance receptor selectivity, induce receptor clustering on cell surfaces, and control signal transduction within cells.[1] A great diversity of biological processes including cell signaling[2] and cell–pathogen interactions[3–5] are associated with multivalent ligand–receptor binding. The recognition of cholera toxin (CT) by ganglioside GM_1 is considered to be a paradigm of multivalent carbohydrate–protein binding.[6] Understanding the underlying physical chemistry of this model system should therefore lead to a better appreciation of multivalent binding phenomena and may provide insight into strategies for inhibitory drug design.[1,3,7,8]

Cholera toxin is a member of the AB_5 class of cytotoxins. It is composed of a catalytically active A subunit and doughnut-shaped homopentameric B subunits that recognize and bind to the pentasaccharide moiety of GM_1 on the cell's membrane. The interaction of cholera toxin or its pentameric B-subunits with GM_1 has been investigated by using a variety of techniques. ^{125}I-labeled CT was first utilized to study binding on isolated fat cells and liver membranes,[9,10] and intestinal cells.[11] Thermodynamic data were obtained by isothermal titration calorimetry.[12,13] Surface plasmon resonance was used to obtain the kinetics of CTB binding to GM_1 in supported bilayers[14,15] and in vesicles.[16,17] Other diagnostic methods used to explore CTB–GM_1 binding include quartz crystal microbalance analysis,[18] flow

cremer@mail.chem.tamu.edu.

Contribution from the Department of Chemistry, Texas A&M University, P.O. Box 30012, College Station, Texas 77843-3012

Supporting Information Available: Experiments concerning the partitioning of GM_1 between the upper and lower POPC bilayer leaflets, binding curves with eight GM_1 concentrations from 0.02 to 10.0 mol % in POPC bilayers, as well as AFM images of GM_1 clustering within POPC bilayers and the corresponding histograms for the size distribution of GM_1 domains. This material is available free of charge via the Internet at http://pubs.acs.org.

cytometry,[19] fluoroimmunoassays,[20] fluorescence resonance energy transfer,[21] atomic force microscopy,[22] and a novel colloid phase transition method.[23,24] The buffer conditions, temperatures, ionic strengths, and membrane chemistries varied among the different experiments. Accordingly, the measured values for the apparent dissociation constant, K_{Dapp}, ranged from 4.55 pM[15] on the low end to 41 nM[23] and even 370 nM[25] on the high end.

In multivalent binding systems ligand density is a key parameter since it affects ligand distribution and interligand distance.[1,3,8,26,27] We previously showed that K_{Dapp} for an antibody–antigen binding system tightened by a factor of ~12 as the ligand density increased from 0.1 to 5.0 mol % in a supported phospholipid membrane.[28] The hapten was a dinitrophenyl (DNP) moiety covalently conjugated to the headgroup of a phospholipid, which was recognized by an anti-DNP IgG. The change in K_{Dapp} with ligand density could be predicted extremely well by taking into account the dissociation constants for the individual steps in a sequential binding model:

$$K_{Dapp} = \frac{K_{D1} K_{D2}}{K_{D2} + 2[L]_s} \quad (1)$$

where K_{D1} and K_{D2} are the equilibrium dissociation constants for the first and second binding events, respectively, and $[L]_s$ is the surface density of the ligands in the lipid bilayer.

Beyond bivalent binding, very little work has been done to probe the effect of membrane ligand density for the binding of proteins with multiple binding pockets. Indeed, the thermodynamics and kinetics of CTB–GM_1 binding have typically been studied at only one or a few ligand densities at a time. Curiously, MacKenzie et al.[16] showed data that indicated approximately 4 times tighter apparent binding of CTB to liposomes containing 2.0 mol % GM_1 than for those containing 4.0 mol % GM_1. Lencer et al.[29] investigated cholera toxin binding to an intestinal microvillus membrane during development, that possessed different GM_1 ligand densities. In that case, the binding also appeared to be stronger at lower ligand density. These results led us to hypothesize that a systematic study of multivalent CTB–GM_1 binding over a range of GM_1 concentrations could reveal that a binding mechanism different from that in the simple case of the bivalent ligand–receptor interaction of the DNP/anti-DNP system was at work.

Herein, a series of binding experiments were performed within microfluidic channels coated with 1-palmitoyl-2-oleoyl-*sn*-glycero-3-phosphocholine (POPC) bilayers containing GM_1. The ganglioside density in the membrane was varied from 0.02 to 10.0 mol %. The results showed that the binding of CTB was continuously weakened as the ligand density was increased. Atomic force microscopy (AFM) studies revealed GM_1 clustering on the phospholipid membranes, which became more pronounced at increased GM_1 densities. On the basis of these observations, it is suggested that CTB binding to GM_1 is inhibited by the clustering of the glycolipid within the phospholipid membrane (Figure 1).

Experimental Section

Materials

Ganglioside GM_1 (brain, ovine-ammonium salt) and POPC were obtained from Avanti Polar Lipids (Alabaster, AL). Texas Red-DHPE and rabbit IgG antibodies were purchased from Molecular Probes, Inc. (Eugene, OR). CTB from *Vibrio cholerae* was purchased from Sigma-Aldrich. The CTB was labeled with Alexa Fluor-594 dye by using a standard protein-labeling kit (A10239, Molecular Probes, Eugene, OR). Labeling yielded ~0.8 fluorophores per protein as determined by UV/vis absorption spectroscopy. The dye-labeled protein was

stored in a phosphate buffered saline (PBS) solution containing 10 mM sodium phosphate, 150 mM NaCl, and 0.2 mM sodium azide. The pH of the PBS was set to 7.2 by dropwise addition of 2.0 M NaOH. The same buffer was also used for vesicle preparation and the successive dilution of protein solutions. Purified water for these experiments came from a NANOpure Ultrapure Water System (18.2 MΩ·cm, Barnstead, Dubuque, IA).

Microfluidic Device Fabrication

We employed microfluidic devices and total internal reflection fluorescence microscopy to study CTB–GM_1 interactions using our previously established methods.[28,30] The devices were made from planar borosilicate glass substrates and lithographically patterned polydimethylsiloxane (PDMS) molds. The devices afforded high throughput capabilities and had extremely low sample consumption compared with traditional analytical tools. Additionally, the glass and PDMS surfaces served as good supports for fluid phospholipid bilayers.[31] Lipid mobility was preserved because a thin water layer (~1 nm thick)[32] was trapped between the phospholipid bilayer and the underlying solid surface. Lipid molecules in the membrane were thus able to diffuse laterally to accommodate multivalent interactions.

The seven-channel microfluidic devices used in these experiments were fabricated by soft lithographic techniques.[30,33] In a first step, microfluidic channels were designed with Corel Draw software (Version 9, Corel Corp.). By printing out the design and transferring it onto black and white high-contrast Kodak technical pan film, the image could be used as a photomask for photolithography. Soda-lime glass slides were cleaned in hot surfactant solution (ICN ×7 detergent, Costa Mesa, CA) for 1 h, rinsed with copious amounts of purified water, and dried with nitrogen gas. Next, the glass slides were coated with a thin layer of hexamethyldisilazane (HMDS) to improve adhesion of the photoresist to the glass surface,[34] followed by spin coating with Shipley 1827 photoresist. The substrates were then exposed to UV light through the photomask and treated with developing solution. After baking the photoresist/glass systems at 120 °C overnight, the substrates were immersed in buffered oxide etchant (BOE) in an ultrasonic bath to etch the glass. After etching, the remaining photoresist was removed with ethanol. PDMS was then poured over the glass masters and cured. The elastomeric molds were carefully peeled off, washed with ethanol and purified water, and dried under a stream of nitrogen. In the penultimate step, the molds were treated in an oxygen plasma for 30 s along with clean planar borosilicate glass substrates. It should be noted that the borosilicate substrates had been previously cleaned in a boiling 1:3 solution of ICN ×7 detergent and purified water. Then the substrates were rinsed with copious amounts of purified water, dried with nitrogen, and annealed in a kiln at 480 °C for 5 h before introduction into the oxygen plasma. Finally, the PDMS molds and glass substrates were brought into contact immediately after oxygen plasma treatment to create finished microfluidic devices.

Preparation of Small Unilamellar Vesicles and Bilayer Formation

Small unilamellar vesicles (SUVs) were prepared by vesicle extrusion.[30,35,36] Lipids dissolved in chloroform were dried under a stream of nitrogen followed by overnight vacuum desiccation. Next, the lipids were rehydrated in PBS buffer (pH 7.2). After five freeze–thaw cycles, the vesicles were extruded more than seven times through a polycarbonate filter (Whatman) containing 50-nm pores. SUVs prepared by this method were 70 ± 10 nm in diameter as determined by dynamic light scattering with a Brookhaven Instruments 90Plus Particle Size Analyzer.

For bilayer formation, 5 μL of a 2.5 mg/mL SUV solution were injected through each inlet port of the linear array microfluidic device. The solution was introduced immediately after plasma treatment and bonding of the PDMS/glass microfluidic platform to ensure that the

surfaces remained hydrophilic. Vesicle fusion occurred on both the PDMS walls and the glass substrate to form a continuous lipid bilayer coating as has been previously reported.[37] The incubation time for bilayer formation was 1 h. The microchannels were rinsed with PBS buffer to remove excess vesicles. Fluorescence recovery after photo-bleaching (FRAP)[38,39] was employed to verify the quality of the supported bilayers on the glass surfaces from which all binding data were obtained.

All solid-supported membranes were made from the fusion of POPC vesicles containing a series of GM_1 concentrations from 0 to 10.0 mol %. The distribution of GM_1 between the upper and lower leaflets of the supported bilayers was tested and found to be the same within experimental error using methods developed by Parikh and coworkers.[40] These data are provided in the Supporting Information. Before the injection of protein solution, the bilayer-coated microchannels were incubated with a 0.5 mg/mL rabbit IgG antibody solution for 30 min to block defect sites in the membrane and thereby suppress nonspecific adsorption of CTB.

Epifluorescence Microscopy and TIRFM

To check the quality and fluidity of supported GM_1/POPC bilayers, FRAP studies were conducted using an inverted epifluorescence Nikon Eclipse TE2000-U microscope with a 10× objective. Laser radiation from a 2.5 W mixed gas Ar^+/K^+ laser (Stabilite 2018, Spectra Physics) was used to bleach the lipid bilayer samples. FRAP images were obtained with a MicroMax 1024b CCD camera (Princeton Instruments). Total internal reflection fluorescence microscopy (TIRFM),[41,42] which can discriminate between dye-labeled CTB molecules bound to the supported membrane and those in the bulk solution, was employed for the determination of binding isotherms. In this case the fluorescence images were obtained with a Nikon E800 fluorescence microscope using a 4× objective. In the TIRFM experiments, a 594-nm helium–neon laser beam (4 mW, Uniphase, Manteca, CA) was passed through a dove prism that was optically coupled to the bottom of the borosilicate substrate of the microfluidic device by index matching immersion oil. Alexa 594-labeled CTB solutions were simultaneously flowed through each channel at various concentrations at a rate of 0.2 μL/min by a Harvard PHD 2000 syringe pump (Harvard Apparatus, Holliston, MA). The helium–neon laser beam was telescoped out by a line generator lens (BK7 for 30°, Edmund Optics, Barrington, NJ) to create a uniform intensity profile across the microchannel array. As the laser illuminated the interface between the bilayer-coated glass substrate and the bulk aqueous solution, it was totally internally reflected, creating an evanescent wave above the interface. The evanescent wave decayed exponentially to its 1/e value by ~70 nm above the interface under the experiment conditions employed here.[30,43] This allowed the proteins bound to the supported lipid bilayer to be studied with high specificity. The TIRFM images were captured with a Micromax 1024b CCD camera, collected using Metamorph software (Universal Imaging Corp.), and transferred to Sigma Plot for further processing. Measurements of thermodynamic binding constants were made only after the fluorescence intensity from the interface reached equilibrium. This took up to 6 h at the lowest protein concentrations.

Atomic Force Microscopy

AFM images of supported lipid bilayers were acquired with a Nanoscope IIIa Multimode SPM (Digital Instruments, Santa Barbara, CA) equipped with a J-type scanner. POPC bilayers samples were probed with 0.0, 0.1, 0.5, 1.0, 3.0, 5.0, and 10.0 mol % GM_1. The experimental conditions were identical to those used in the microfluidic devices except for the fact that the PDMS mold above the glass surface was absent. Instead, the bilayer-coated borosilicate glass served as the bottom of a standard AFM liquid sample cell. All images were obtained in fluid contact mode at a scan rate of 2.0 Hz using oxide-sharpened DNP-S1

silicon nitride probes (spring constant: 0.06 N/m; Veeco Probes, Santa Barbara, CA). The only treatment applied to the images was flattening. GM_1 domains were judged to be present on the POPC bilayer surface when the feature height exceeded 1.0 nm above the membrane background. In this case, the nominal width of a domain was taken from the point where the feature height first began to rise above the background level and ended when it returned to background level. To abstract more quantitative information on the GM_1 cluster size, a standard deconvolution method was employed.[44,45] For this purpose a nominal AFM tip radius of 10 nm was assumed (according to the manufacturer's specifications), and a headgroup height of 1.0 nm for the GM_1 features was also employed. Under these conditions, the sizes of the GM_1 clusters, which had nominal mean diameters between 16.1 and 28.3 nm, were reduced by 8.8 nm to take tip–sample convolution effects into account.

Results

A schematic representation of the lipid-coated PDMS microchannels bonded to a planar glass support is shown in Figure 2a. GM_1/POPC bilayers were coated over the entire surface (shown in green). The surface binding process was monitored by TIRFM as a function of time until the fluorescence intensity remained constant. A typical TIRF image is shown in Figure 2b. In this case the bulk CTB concentration ranged from 6.0 to 0.090 nM (left to right). Control experiments were conducted under the same conditions without GM_1 in the POPC membrane. Under these conditions, virtually no background fluorescence signal was observed, as the bulk protein concentrations were so low.[19,22] Intensity profiles across the TIRF image (dotted red line in Figure 2b) were employed to obtain quantitative binding data.

In a first set of experiments, solid-supported POPC bilayers containing 0.05, 0.5, and 5.0 mol % GM_1 were prepared in separate parallel arrays of microfluidic channels and tested for CTB binding (Figure 3). In order to abstract equilibrium dissociation constants, the CTB–GM_1 binding curves were fit to both the Langmuir isotherm (eq 2) and Hill–Waud (eq 3) binding models:[29]

$$F = F_{\max} \times \frac{[P]}{K_d + [P]} \quad (2)$$

$$F = F_{\max} \times \frac{([P])^n}{(K_H)^n + ([P])^n} \quad (3)$$

where F is the fluorescence intensity from surface-bound proteins, $F_{\max}$ is the maximum fluorescence intensity when proteins completely saturate the bilayer surface, $[P]$ is the bulk CTB concentration, K_d and K_H are the apparent equilibrium dissociation constants for the respective models, and n is the Hill coefficient of cooperativity.[29] The Langmuir isotherm model[46,47] is valid for pentavalent CTB binding to multiple ligands on the surface so long as the individual binding events are independent.[16,18,24] On the other hand, the Hill–Waud model takes into account binding cooperativity by introducing the Hill coefficient, n.[25,29] The Langmuir isotherm fits became progressively poorer as the concentration of surface-bound ligands was increased. In fact, the Hill–Waud model (regression coefficient, R^2 = 0.99) more closely fit the CTB binding data in comparison to the Langmuir adsorption isotherm (R^2 = 0.96) at the highest glycolipid concentration. The apparent dissociation constants K_d (0.69 ± 0.11 nM) and K_H (0.50 ± 0.07 nM) were also somewhat different under these circumstances.

Experiments similar to those shown in Figure 3 were performed at eight GM_1 concentrations ranging from 0.02 to 10.0 mol % in POPC bilayers. All binding curves are shown in the Supporting Information. The fits to the Hill–Waud and Langmuir binding models are provided in Table 1. As can be seen, as the GM_1 density was increased, the Hill coefficient, n, deviated ever further from 1.0 and K_H became significantly different from K_d. At the lowest GM_1 density, however, K_d and K_H were indistinguishable within experimental error and the Hill coefficient approached 1.0. This suggests that CTB binds cooperatively to GM_1 at high ligand densities. Such a finding is in agreement with previous observations.[12,13,25,29] More significantly, the apparent equilibrium dissociation constant continuously weakened with increasing ligand density.

The K_H values as a function of GM_1 concentration in the POPC bilayer from Table 1 are plotted in Figure 4. As can be seen, the data do not show a linear trend as a function of ligand density. Rather, the apparent dissociation constant weakens more sharply as a function of concentration at low GM_1 concentrations, but begins to level out at higher concentrations. The curve shape is reminiscent of a binding isotherm. Two possible origins for this phenomenon need to be considered. First, one might hypothesize that the weakening of the binding could be caused by clustering of the GM_1 lipids. Alternatively, the weakening of K_H might be the result of electrostatic repulsion between the negatively charged CTB and the increasingly negatively charged membrane as the ligand density is increased (note: each GM_1 headgroup has a charge of −1).[15]

To investigate GM_1 clustering, AFM experiments were performed as a function of GM_1 concentration in supported POPC bilayers in the absence of CTB. A pure POPC membrane was imaged first as a control (Figure 5a). As expected, the membrane looked relatively flat and featureless. By contrast, systems containing 0.5 mol % GM_1 (Figure 5b) and 5.0 mol % GM_1 (Figure 5c) contained ~1.0–2.0 nm high features which are consistent with the presence of GM_1.[48] In fact, the height of the GM_1 pentasacchride headgroup has been measured by X-ray diffraction and is consistent with this finding.[49,50] AFM images of POPC bilayers containing 0.1, 1.0, 3.0, and 10.0 mol % GM_1 are provided in the Supporting Information. The apparent size of the domains in these images ranged from approximately 15 to 60 nm. Consistent with expectations, these domains were more prevalent at high GM_1 density (e.g., 5.0 mol %) than at low density (e.g., 0.5 mol %).

To quantify the domain size distribution in the POPC bilayers, the approximate diameter of the GM_1 domains were measured and counted from four independent 500 nm × 500 nm AFM micrographs at each ligand density. Histograms for the number of GM_1 domains as a function of apparent cluster size at 0.5 mol % and 5.0 mol % are provided in Figure 6. Additional histograms for GM_1 densities between 0.1 mol % and 10.0 mol % are provided in the Supporting Information. As can be seen from Figures 5 and 6, GM_1 clustering within the POPC bilayers became more pronounced at increased GM_1 densities. The mean domain size after deconvolution at 0.5 mol % was 11.0 nm, and this value rose to 18.6 nm for 5.0 mol % GM_1. In fact, the mean domain size continually shifted from ~7 nm to ~20 nm as the GM_1 density was increased from 0.1 mol % to 10.0 mol % (Table 2).

To further elucidate the binding mechanism as a function of ligand density, the shape of the K_H vs GM_1 ligand density curve shown in Figure 4 needs to be considered. As mentioned above, the curve shape is reminiscent of a binding isotherm. Treating the curve in this manner requires that the y-axis be considered in a fashion analogous to a fractional coverage of available sites. This was achieved by fitting the data in Figure 4 to a binding isotherm equation:

$$y=y_0+y_{max}x/(b+x) \quad (4)$$

This allows the y intercept (y_0 at $x = 0$) and the maximum value (y_{max} at $x = \infty$) to be obtained. By offsetting y_0 to 0 and normalizing y_{max} to equal 1, the y-axis essentially becomes analogous to a surface coverage. On the other hand, the x-axis must be treated as a two-dimensional concentration. This can be done by noting that 1.0 mol % GM_1 is equivalent to a number density of 0.237 nmol/dm^2 (assuming an average area per POPC lipid of ~0.7 nm^2).[51] Number density units of square decimeters rather than square meters are employed in analogy to molar units which are mol/dm^3. Doing this produces an equation in the form:

$$f=\frac{[L]_s}{B_s+[L]_s} \quad (5)$$

where f is a unitless fraction which ranges from 0 to 1. $[L]_s$ is the two-dimensional number density of the glycolipid. The subscript, s, is used to denote the fact that this is a surface concentration. B_s is the apparent two-dimensional dissociation constant which also has units of mol/dm^2. The value of f approaches zero if all of the glycolipids are separated from one another and reaches 1.0 when they are completely clustered. A fit to the data is shown in Figure 7a. The abstracted parameter, B_s = 0.50 nmol/dm^2, is a remarkably good fit to the data (R^2 = 0.99). This would imply that half of the ganglioside molecules are clustered at 2.1 mol % GM_1 in the POPC membrane.

The abstracted value of B_s for GM_1 clustering should be compared with the AFM data in Table 2. To do this, the square of the mean domain diameter, Φ^2, is plotted as a function of GM_1 density in Figure 7b. Φ^2 was chosen instead of Φ because it is proportional to the area of the GM_1 domains and, hence, to the number of glycolipids. By fitting the domain area data to a Langmuir isotherm, a nominal equilibrium dissociation constant for GM_1 clustering on the POPC bilayer can be extracted. The result gives an apparent value of K_d = ~1.4 mol % GM_1 for the AFM data, which is a rather close match to the results in Figure 7a. This is strong evidence that GM_1 clustering is correlated to the observed weakening of the equilibrium dissociation constant for the CTB–GM_1 system as a function of glycolipid density.

Although, the clustering hypothesis is consistent with the AFM results, an electrostatic repulsion hypothesis was also considered to explain the data in Figure 4. It should be noted, however, that an electrostatic effect seems implausible on several grounds. First, electrostatic repulsion between the negatively charged GM_1 glycolipids and the CTB proteins would probably not be expected to show the type of saturation behavior found in Figure 4. Moreover, the Debye length is already rather short at the salt concentration employed in these experiments (~0.8 nm for 150 mM NaCl).[52] This means that an incoming CTB molecule should not experience significant electrostatic repulsion from the charge on the membrane.

Nevertheless, we wished to test the electrostatic hypothesis. To do this, we monitored CTB binding in the presence of PBS buffer with a higher NaCl concentration (300 mM). Under these conditions one might expect the apparent dissociation constant to tighten if electrostatic repulsion were playing a significant role in the effects observed in Figure 4. Our results, however, showed no evidence for a change in the binding constant at higher salt concentration. This was true even when 10.0 mol % GM_1 was present in the membrane. In fact, K_H was measured to be 0.62 nM for 10.0 mol % GM_1 in the presence of 300 mM NaCl. This value is identical within experimental error to the value obtained in Table 1 with

150 mM NaCl (0.59 nM). Illustrative data are shown in Figure 8. This plot shows the line profile of the fluorescence intensity across a seven-channel microfluidic device containing POPC membranes with 10.0 mol % GM_1. The first three channels show data at various concentrations of CTB in the presence of PBS buffer with 300 mM NaCl, while the last three channels are for the identical conditions, but employing buffer with 150 mM NaCl. As can be seen, the fluorescence intensities are virtually unaffected by the increase in salt.

Discussion

The effect of ligand density on CTB–GM_1 binding presented here is opposite to that which would be predicted by a simple noncooperative sequential binding model (eq 1). In the absence of interacting ligands, steric/allosteric effects, or other related phenomena, one would expect that increasing ligand density at the membrane interface would strengthen ligand–receptor binding as was previously found in the case of antibody–antigen interactions.[28] Herein, however, increased GM_1 density in the phospholipid membrane actually led to a weakening of the apparent equilibrium binding constant. This effect is almost certainly caused by interactions between the ganglioside molecules, which induced GM_1 clustering on the solid-supported phospholipid membranes.

The crystal structure of the CT–GM_1 binding complex has been investigated by Merritt,[53] and isothermal titration calorimetry investigations have been performed by Turnbull.[54] These studies show that the binding-site specificity of cholera toxin for GM_1 arises from recognition of the sialic acid, terminal galactose, and *N*-acetylgalactosamine moieties. Specifically, the majority of CTB–GM_1 interactions involve hydrogen bonds (H-bonds) to the sugar hydroxyl groups. The clustering found in our AFM images suggests that at least some of these moieties may be involved in H-bond formation with neighboring GM_1 molecules. This idea is further supported by electron paramagnetic resonance spectroscopy experiments of GM_1 in phospholipid membranes, which indicated that the oligosaccharide head group is capable of forming intermolecular H-bonds.[55] Hydrogen bonding between membrane-bound GM_1 molecules in model membranes has also been suggested on the basis of freeze–etch electron microscopy.[56] In the present experiments, such lateral interactions should effectively compete with the binding of the CTB proteins. Moreover, the crowding of the GM_1 molecules may limit CTB binding on steric grounds. The putative mechanism for these effects is presented in Figure 1.

It is interesting to note that previous studies have concluded that GM_1-enriched lipid raft domains are needed to ensure maximal binding of CT to the cell surface.[57,58] Wolf et al.[59] proposed that toxin-induced signal transduction depends on the coupling of CT with GM_1-enriched caveolae or caveolae-like membrane domains. No results to date, however, have shown stronger binding of CT to GM_1-enriched raft domains. The results in this paper indicate that GM_1 domain clustering may not strengthen toxin–ligand interactions. Rather, higher GM_1 concentrations would simply lead to greater number densities of toxin molecules bound in these locations. It should be noted, however, that cell membranes typically included other lipids such as sphingolipids and cholesterol which could possibly play a role in GM_1 presentation and, hence, in the thermodynamics of cholera toxin binding.

Conclusion

Systematic studies of multivalent CTB–GM_1 interactions were undertaken as a function of ligand density by using a microfluidic strategy in conjunction with TIRFM. CTB bound more weakly at higher ligand densities, and this observation was ascribed to the clustering of GM_1 in the phospholipid bilayer. AFM results supported this hypothesis. Furthermore,

characteristic equilibrium dissociation constant measurements for GM_1 clustering on solid-supported phospholipid membranes were determined.

Supplementary Material

Refer to Web version on PubMed Central for supplementary material.

Acknowledgments

We thank the National Institutes of Heath (R01-070622) for support.

References

1. Choi, SK. Synthetic Multivalent Molecules. Wiley; Hoboken, NJ: 2004.
2. Heldin CH. Cell. 1995; 80:213–223. [PubMed: 7834741]
3. Mammen M, Choi SK, Whitesides GM. Angew Chem, Int Ed. 1998; 37:2755–2794.
4. Kiessling LL, Pohl NL. Chem Biol. 1996; 3:71–77. [PubMed: 8807830]
5. Baranowski E, Ruiz-Jarabo CM, Domingo E. Science. 2001; 292:1102–1105. [PubMed: 11352064]
6. Keizer J. Acc Chem Res. 1985; 18:235–241.
7. Mourez M, Kane RS, Mogridge J, Metallo S, Deschatelets P, Sellman BR, Whitesides GM, Collier RJ. Nat Biotechnol. 2001; 19:958–961. [PubMed: 11581662]
8. Kiessling LL, Gestwicki JE, Strong LE. Angew Chem, Int Ed. 2006; 45:2348–2368.
9. Cuatreca P. Biochemistry. 1973; 12:3547–3558. [PubMed: 4731191]
10. Cuatreca P. Biochemistry. 1973; 12:3558–3566. [PubMed: 4731192]
11. Holmgren J, Lonnroth I, Mansson JE, Svennerholm L. Proc Natl Acad Sci USA. 1975; 72:2520–2524. [PubMed: 1058471]
12. Goins B, Freire E. Biochemistry. 1988; 27:2046–2052. [PubMed: 3378043]
13. Schon A, Freire E. Biochemistry. 1989; 28:5019–5024. [PubMed: 2765522]
14. Terrettaz S, Stora T, Duschl C, Vogel H. Langmuir. 1993; 9:1361–1369.
15. Kuziemko GM, Stroh M, Stevens RC. Biochemistry. 1996; 35:6375–6384. [PubMed: 8639583]
16. MacKenzie CR, Hirama T, Lee KK, Altman E, Young NM. J Biol Chem. 1997; 272:5533–5538. [PubMed: 9038159]
17. Cooper MA, Hansson A, Lofas S, Williams DH. Anal Biochem. 2000; 277:196–205. [PubMed: 10625506]
18. Janshoff A, Steinem C, Sieber M, el Baya A, Schmidt MA, Galla HJ. Eur Biophys J. 1997; 26:261–270. [PubMed: 9273995]
19. Lauer S, Goldstein B, Nolan RL, Nolan JP. Biochemistry. 2002; 41:1742–1751. [PubMed: 11827518]
20. Singh AK, Harrison SH, Schoeniger JS. Anal Chem. 2000; 72:6019–6024. [PubMed: 11140771]
21. Ma GY, Cheng Q. Langmuir. 2006; 22:6743–6745. [PubMed: 16863214]
22. Cai XE, Yang J. Biochemistry. 2003; 42:4028–4034. [PubMed: 12680755]
23. Baksh MM, Jaros M, Groves JT. Nature. 2004; 427:139–141. [PubMed: 14712272]
24. Winter EM, Groves JT. Anal Chem. 2006; 78:174–180. [PubMed: 16383325]
25. Moran-Mirabal JM, Edel JB, Meyer GD, Throckmorton D, Singh AK, Craighead HG. Biophys J. 2005; 89:296–305. [PubMed: 15833994]
26. Smith EA, Thomas WD, Kiessling LL, Corn RM. J Am Chem Soc. 2003; 125:6140–6148. [PubMed: 12785845]
27. Huskens J, Mulder A, Auletta T, Nijhuis CA, Ludden MJW, Reinhoudt DN. J Am Chem Soc. 2004; 126:6784–6797. [PubMed: 15161307]
28. Yang TL, Baryshnikova OK, Mao HB, Holden MA, Cremer PS. J Am Chem Soc. 2003; 125:4779–4784. [PubMed: 12696896]
29. Lencer WI, Chu SH, Walker WA. Infect Immunol. 1987; 55:3126–3130. [PubMed: 3679546]

30. Yang TL, Jung SY, Mao HB, Cremer PS. Anal Chem. 2001; 73:165–169. [PubMed: 11199961]
31. Sackmann E. Science. 1996; 271:43–48. [PubMed: 8539599]
32. Johnson SJ, Bayerl TM, Mcdermott DC, Adam GW, Rennie AR, Thomas RK, Sackmann E. Biophys J. 1991; 59:289–294. [PubMed: 2009353]
33. Xia YN, Whitesides GM. Angew Chem, Int Ed. 1998; 37:551–575.
34. Lin CH, Lee GB, Lin YH, Chang GL. J Micromech Microeng. 2001; 11:726–732.
35. Kalb E, Frey S, Tamm LK. Biochim Biophys Acta. 1992; 1103:307–316. [PubMed: 1311950]
36. Nollert P, Kiefer H, Jahnig F. Biophys J. 1995; 69:1447–1455. [PubMed: 8534815]
37. Mao HB, Yang TL, Cremer PS. Anal Chem. 2002; 74:379–385. [PubMed: 11811412]
38. Axelrod D, Koppel DE, Schlessinger J, Elson E, Webb WW. Biophys J. 1976; 16:1055–1069. [PubMed: 786399]
39. Albertorio F, Diaz AJ, Yang TL, Chapa VA, Kataoka S, Castellana ET, Cremer PS. Langmuir. 2005; 21:7476–7482. [PubMed: 16042482]
40. Howland MC, Sapuri-Butti AR, Dixit SS, Dattelbaum AM, Shreve AP, Parikh AN. J Am Chem Soc. 2005; 127:6752–6765. [PubMed: 15869298]
41. Axelrod D, Burghardt TP, Thompson NL. Annu Rev Biophys Bioeng. 1984; 13:247–268. [PubMed: 6378070]
42. Starr TE, Thompson NL. Biophys J. 2001; 80:1575–1584. [PubMed: 11222318]
43. Burmeister JS, Olivier LA, Reichert WM, Truskey GA. Biomaterials. 1998; 19:307–325. [PubMed: 9677147]
44. Doudevski I, Schwartz DK. Phys Rev B. 1999; 60:14–17.
45. Losic D, Short K, Gooding JJ, Shapter JG. J Serb Chem Soc. 2004; 69:93–106.
46. Pisarchick ML, Thompson NL. Biophys J. 1990; 58:1235–1249. [PubMed: 2291943]
47. Kalb E, Engel J, Tamm LK. Biochemistry. 1990; 29:1607–1613. [PubMed: 2334720]
48. Yuan CB, Johnston LJ. Biophys J. 2001; 81:1059–1069. [PubMed: 11463647]
49. Mcintosh TJ, Simon SA. Biochemistry. 1994; 33:10477–10486. [PubMed: 8068686]
50. Mcdaniel RV, Mcintosh TJ. Biophys J. 1986; 49:94–96. [PubMed: 19431664]
51. White SH, King GI. P Natl Acad Sci USA. 1985; 82:6532–6536.
52. Israelachvili, JN. Intermolecular and Surface Forces. 2. Academic Press; San Diego, CA: 1991.
53. Merritt EA, Sarfaty S, Vandenakker F, Lhoir C, Martial JA, Hol WGJ. Protein Sci. 1994; 3:166–175. [PubMed: 8003954]
54. Turnbull WB, Precious BL, Homans SW. J Am Chem Soc. 2004; 126:1047–1054. [PubMed: 14746472]
55. Sharom FJ, Grant CWM. Biochim Biophys Acta. 1978; 507:280–293. [PubMed: 203316]
56. Peters MW, Grant CWM. Biochim Biophys Acta. 1984; 775:273–282. [PubMed: 6547854]
57. Fantini, J.; Garmy, N.; Mahfoud, R.; Yahi, N. Lipid Rafts: Structure, Function and Role in HIV, Alzheimer's and Prion Diseases. Cambridge University Press; UK: 2002.
58. van der Goot FG, Harder T. Semin Immunol. 2001; 13:89–97. [PubMed: 11308292]
59. Wolf AA, Jobling MG, Wimer-Mackin S, Ferguson-Maltzman M, Madara JL, Holmes RK, Lencer WI. J Cell Biol. 1998; 141:917–927. [PubMed: 9585411]

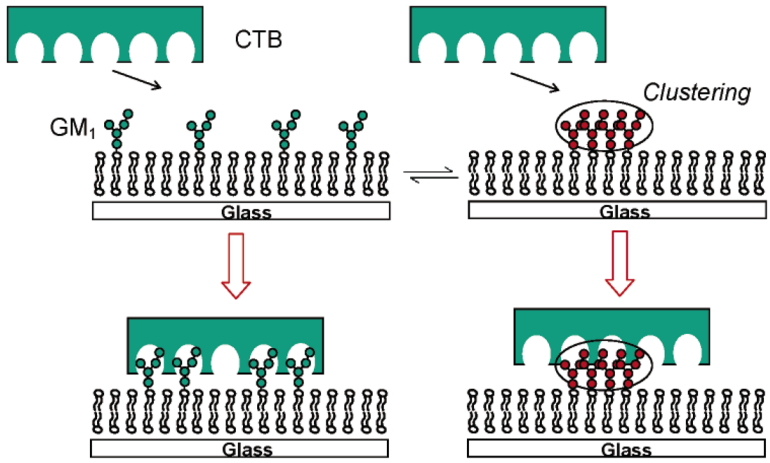

Figure 1.
Schematic representation of the inhibition of CTB binding by GM_1 clustering on supported POPC bilayers. For simplicity GM_1 molecules in the lower leaflet are not drawn.

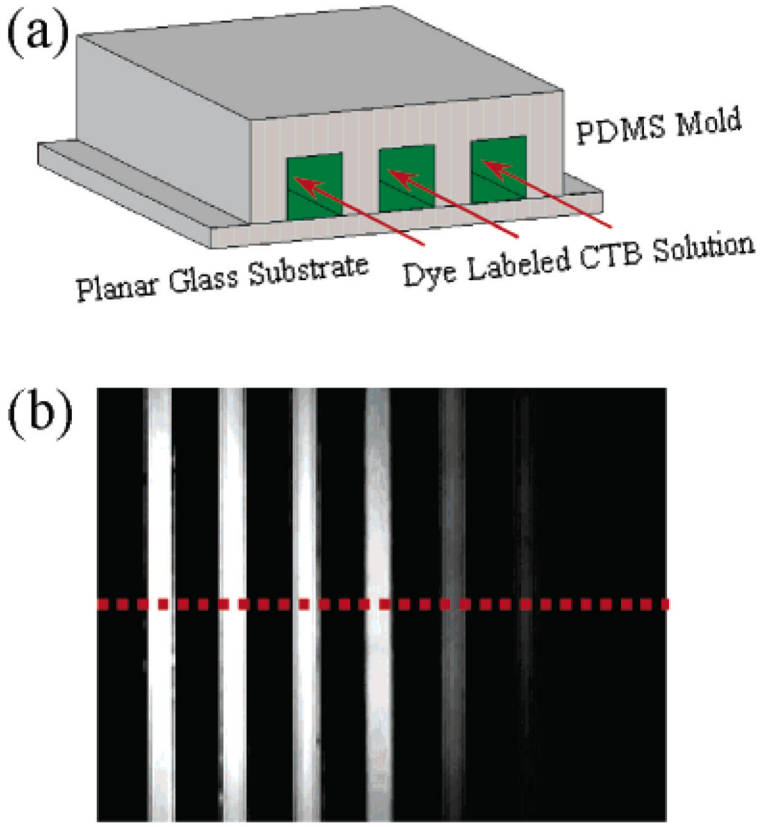

Figure 2.
(a) Schematic representation of bilayer-coated PDMS/glass microchannels. (b) TIRF image of a bilayer-coated microchannel array containing various concentrations of dye-labeled CTB.

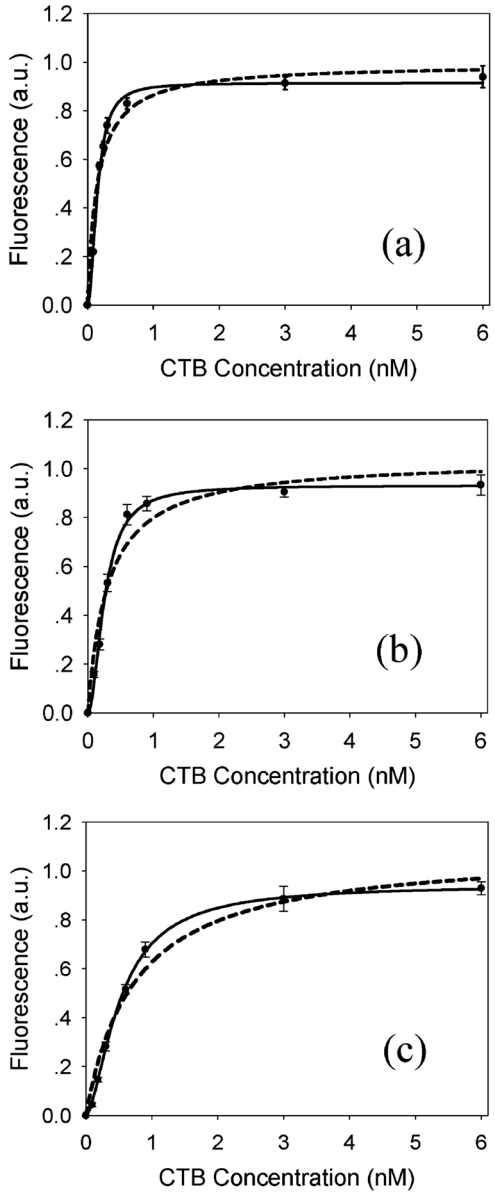

Figure 3.

TIRF intensity of surface-bound CTB vs bulk protein concentration at three different GM_1 densities in POPC bilayers: (a) 0.05 mol %, (b) 0.5 mol %, and (c) 5.0 mol %. The dashed curves were fits to a Langmuir adsorption isotherm, while the solid curves were fits to the Hill–Waud model.

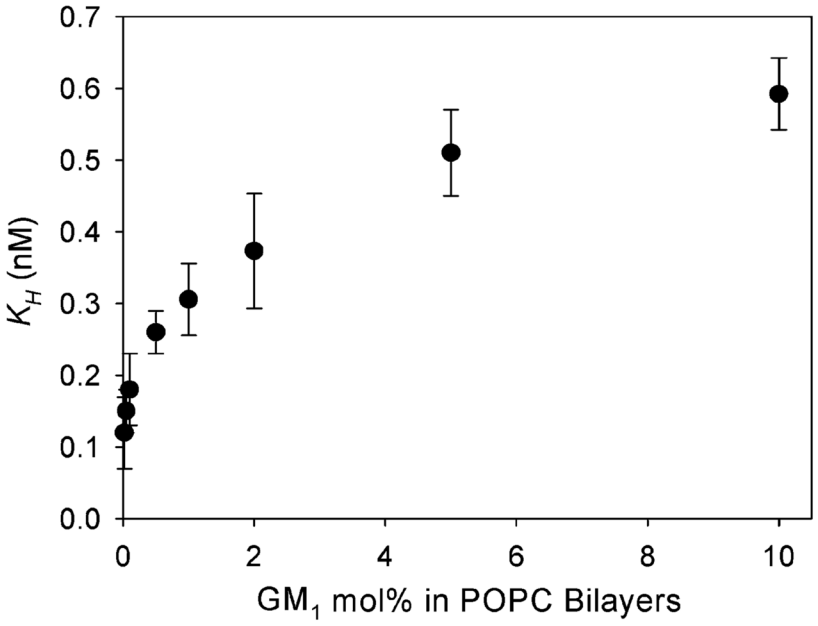

Figure 4.
K_H vs the concentration of GM_1 in the POPC bilayers for CTB–GM_1 binding.

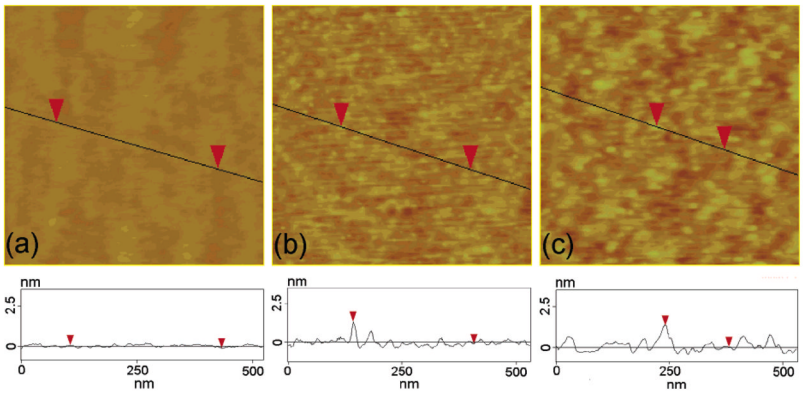

Figure 5.

AFM images of GM_1 clustering on POPC bilayers: (a) a pure POPC bilayer, (b) a POPC bilayer containing 0.5 mol % GM_1, and (c) a POPC bilayer containing 5.0 mol % GM_1. Each image is 500 nm × 500 nm.

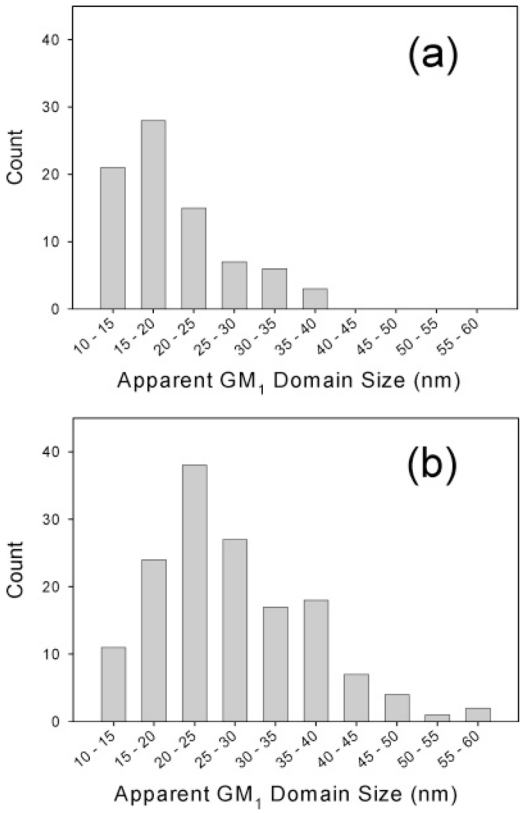

Figure 6.

Histograms for the distribution of GM_1 domains within POPC bilayers: (a) 0.5 mol % and (b) 5.0 mol % GM_1. There were a total of 80 counts for the 0.5 mol % bilayer and 149 counts at 5.0 mol %.

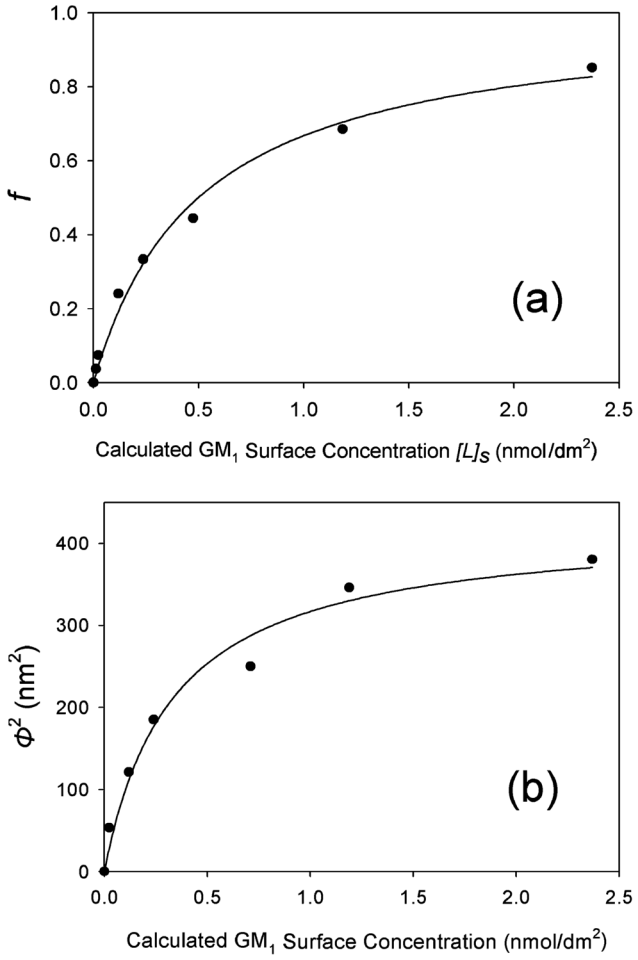

Figure 7.
Fitted plots of (a) *f* and (b) the square of characteristic domain size, (Φ^2), vs the GM_1 surface concentration in POPC membranes.

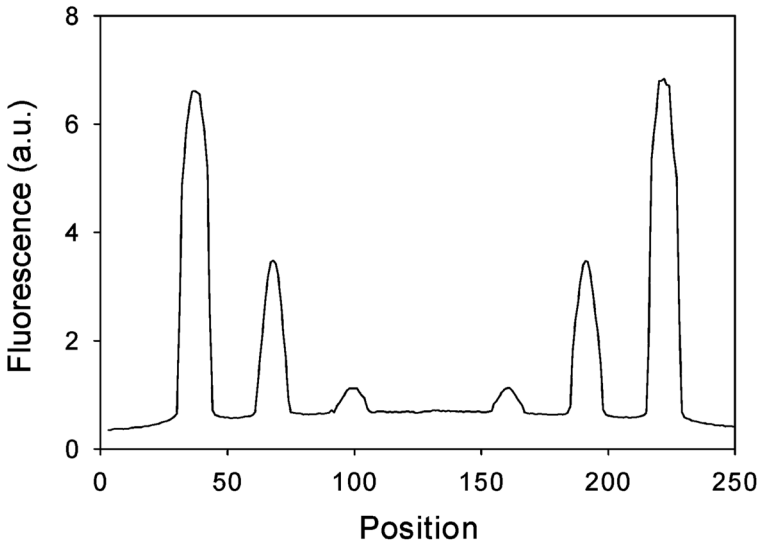

Figure 8.

Line profile of the TIRF intensity across a seven-channel, bilayer-coated microfluidic device containing 10.0 mol % GM_1. Solutions containing 6.0 nM, 0.6 nM, and 0.12 nM CTB were made containing 300 mM NaCl. These solutions were flowed through the first three channels, respectively. Similar samples in the reverse order with 150 mM NaCl were flowed through the last three channels. The channel in the middle was filled with PBS buffer and used as a reference for determining the background level.

Table 1

[GM_1] (mol %) in POPC bilayers	K_d (nM)	K_H (nM)	*n*
0.02	0.11 ± 0.07	0.11 ± 0.05	1.3
0.05	0.16 ± 0.05	0.15 ± 0.03	1.6
0.1	0.23 ± 0.10	0.17 ± 0.06	1.5
0.5	0.32 ± 0.07	0.26 ± 0.04	1.8
1.0	0.39 ± 0.08	0.31 ± 0.05	1.9
2.0	0.46 ± 0.15	0.37 ± 0.10	1.9
5.0	0.69 ± 0.11	0.50 ± 0.07	2.0
10.0	0.86 ± 0.09	0.59 ± 0.05	2.0

Table 2

GM_1 mol %	calcd GM_1 surface concn (nmol/dm^2)	apparent mean size (nm)	mean size after deconvolution (nm)
10.0	2.37	28.3	19.5
5.0	1.19	27.4	18.6
3.0	0.71	24.1	15.3
1.0	0.24	22.4	13.6
0.5	0.12	19.8	11.0
0.1	0.024	16.1	7.3